

Hamiltonian intermittency and Lévy flights in the three-body problem

Ivan I. Shevchenko*

Pulkovo Observatory of the Russian Academy of Sciences

Pulkovskoje ave. 65, St.Petersburg 196140, Russia

Abstract

We consider statistics of the disruption and Lyapunov times in an hierarchical restricted three-body problem. We show that at the edge of disruption the orbital periods and the size of the orbit of the escaping body exhibit Lévy flights. Due to them, the time decay of the survival probability is heavy-tailed with the power-law index equal to $-2/3$, while the relation between the Lyapunov and disruption times is quasilinear. Applicability of these results in an “hierarchical resonant scattering” setting for a three-body interaction is discussed.

Key words: three-body problem, Hamiltonian dynamics, chaotic dynamics, Kepler map, Lyapunov exponents.

*E-mail: iis@gao.spb.ru

1 Introduction

Notwithstanding a three-centennial progress in the studies of the three-body problem, disruption of a three-body gravitational system still remains an enigmatic dynamical process. The statistics of the disruption times is of special interest. In particular, it is interesting whether the computed Lyapunov exponents of the motion are related in some way to the disruption times or, more generally, to the times of sudden changes in the orbital behavior. (The inverse of the maximum Lyapunov exponent, — the Lyapunov time T_L , gives the timescale of exponential divergence of close trajectories in phase space; it characterizes the level of predictability of the motion. The disruption time T_d is the system lifetime as a bound system.)

Much numerical-experimental work has been done on this subject in the last two decades. A prominent relationship in the statistics of sudden orbital changes in gravitational systems has been found and confirmed. This relationship consists in the close-to-quadratic character of the dependence of the time T_r of a sudden orbital change on the Lyapunov time T_L . (The time of a sudden orbital change is dynamically equivalent to the recurrence time for entering some domain in the phase space of a Hamiltonian system, therefore it is designated T_r here and in the following.) On the basis of extensive numerical experiments in the dynamics of three-body and more complicated gravitational systems (in particular, in asteroidal dynamics), it was argued in [1, 2, 3] that the time T_r could be statistically predicted by means of computation of the maximum Lyapunov exponent. A simple “universal” statistical relationship was established to exist between the computed time T_r and the computed Lyapunov time T_L (the inverse of the computed maximum Lyapunov exponent):

$$T_r \propto T_L^\beta \tag{1}$$

with $\beta = 1.7$ – 1.8 typically, though considerable dispersion of the statistical data was usually present. The same kind of relationship with $\beta \approx 1.9$ was found in [4] in simulations of the dynamics of the Kuiper belt of asteroids. Similar dependences were found in [5, 6] for the chaotic behavior of asteroids moving close to the mean motion resonances $2/1$ and $3/1$ with Jupiter. Tsiganis et al. [7] studied chaotic diffusion and effective stability of Jupiter Trojans, and in a large chaotic region, surrounding the stability zone in the motion of asteroids in the Trojan swarms, obtained a statistical relationship

between the escape and Lyapunov times, similar to the “universal” close-to-quadratic one.

However, recent numerical-experimental statistical studies [8, 9] of the disruption process in three-body systems revealed a new — quasilinear — kind of relation between the Lyapunov times and the disruption times. Mikkola and Tanikawa [8] explored correlation of the Lyapunov times T_L and the disruption times T_d in the equal-mass three-body problem. In extensive numerical experiments they computed the disruption and Lyapunov times for the motion with randomized initial conditions, and showed that the system lifetimes, as a bound triple, and the Lyapunov times were correlated, the “ $T_L - T_d$ ” relationship at long lifetimes being close to linear. Urmitsky and Heggie [9] explored correlation between the Lyapunov and disruption times in an hierarchical three-body problem in a setting of the three-body problem different from that used in [8], but obtained similar results. Namely, they considered the Sitnikov problem [10] and, as an outcome of extensive numerical experiments, obtained a two-part power-law relationship with the second part (tail) close to linear one, similar to that found in [8] for the equal-mass three-body problem.

Though the results [8, 9] on the “ $T_L - T_d$ ” relationship are similar, they diverge significantly from the earlier results [1, 2, 3, 4, 5, 6, 7] obtained for the statistics of sudden orbital changes.

In this paper we identify causes that lead to the quasilinear “ $T_L - T_d$ ” relationship in the three-body problem at the edge of disruption, as opposed to the earlier found close-to-quadratic “ $T_L - T_r$ ” dependence in resonant dynamics, and explain its nature as an effect of Hamiltonian intermittency.

2 Two kinds of Hamiltonian intermittency

The close-to-quadratic relationship (1) between the recurrence and Lyapunov times in general Hamiltonian systems with divided phase space (i.e., with regular and chaotic kinds of motion both present) has a straightforward explanation if one takes into account the so-called “stickiness phenomenon” [6, 11]: the correlation arises because the trajectories sticking to chaos border have large recurrence times (the times of return to some domain of phase space), and, since they mimic regular ones, they have also large computed (“local”) Lyapunov times. The relationship between the recurrence time T_r

and the local Lyapunov time T_L on each recurrence was shown to be close to quadratic [6]:

$$T_r \propto T_L^2, \quad (2)$$

i.e., $\beta \approx 2$ in Eq. (1). This relationship was derived in [6] for the motion inside the chaotic layer near the separatrices of nonlinear resonance in the perturbed pendulum model, and this indeed covers a lot of possible applications, including the chaotic motion of asteroids near mean motion resonances. The separatrix map theory [12, 13, 14] was used for deriving relation (2).

Generally speaking, the emergence of the algebraic “ $T_L - T_r$ ” relationship is due to Hamiltonian intermittency. The phenomenon of intermittency, i.e., chaotic behavior intermittently interchanged with close-to-regular one, is well known in studies of dissipative dynamical systems [14]. Much less it is discussed in connection with Hamiltonian dynamics. There are two kinds of Hamiltonian intermittency known. The first one [15] takes place when the motion is “stochastized” at encounters with the separatrix, while most of the time (far from the separatrix) the motion looks regular. The separatrix in the simple model [15], as well as in the map models (4, 5) considered in this paper, is just the singular line $y = 0$ separating bound and unbound types of motion. The first kind Hamiltonian intermittency is inherent to adiabatic chaos; see [16, 17] and references therein. The second kind Hamiltonian intermittency [18] takes place when a fractal “chaos–order” boundary is present in phase space. Sticking to the border results in long time segments of close-to-regular behavior; they are interrupted by prominently chaotic dynamical events, when the trajectory leaves the border neighborhood [19, 20, 6, 18]. Thus the physical cause for the Hamiltonian intermittency of the first kind consists in close encounters of a trajectory with slowly pulsating separatrix, while the physical cause for that of the second kind consists in sticking of a trajectory to chaos border. Statistical properties of these two kinds of phenomena are very different, as demonstrated further in this paper. This is just the second kind Hamiltonian intermittency that is responsible for the quadratic “ $T_L - T_r$ ” relationship (2) [6]. In what follows we show that in certain circumstances a quasilinear “ $T_L - T_r$ ” relationship can arise, and this is due to the first kind Hamiltonian intermittency.

3 General separatrix maps

The nonlinear pendulum provides a model of nonlinear resonance under definite conditions [12, 14]. The motion in the vicinity of the separatrix of the nonlinear pendulum (nonlinear resonance) is described by the separatrix map [12, 14]. We write it in the form adopted in [6]:

$$\begin{aligned} y_{i+1} &= y_i + \sin x_i, \\ x_{i+1} &= x_i + \lambda \ln |y_{i+1}| + c, \end{aligned} \tag{3}$$

where y denotes the normalized relative pendulum's energy, x is normalized time, the constants λ and c are parameters.

Consider a map similar to the separatrix map (3), but with a power-law phase increment instead of the logarithmic one:

$$\begin{aligned} y_{i+1} &= y_i + \sin x_i, \\ x_{i+1} &= x_i + \lambda |y_{i+1}|^{-\gamma}, \end{aligned} \tag{4}$$

or, in an equivalent form usually used,

$$\begin{aligned} w_{i+1} &= w_i + W \sin \tau_i, \\ \tau_{i+1} &= \tau_i + \kappa |w_{i+1}|^{-\gamma}. \end{aligned} \tag{5}$$

Map (5) has two parameters, W and κ , instead of one parameter λ in map (4); apart from the γ parameter. The two-parameter map (5) is reduced to the one-parameter map (4) with $\lambda = \kappa W^{-\gamma}$ by means of straightforward substitution $w = Wy$, $\tau = x$.

A number of mechanical and physical models are described by maps (4) and (5) with rational values of γ . The values of $\gamma = 1/4$ and $1/3$ correspond to the Markeev maps [21, 22] for the motion near separatrices of resonances in two degenerate cases; $\gamma = 1/2$ gives the “ \hat{L} -map” [15] for the motion of a non-relativistic particle in the field of a wave packet, this value of γ also gives a map for the classical Morse oscillator driven by time-periodic force [23]; $\gamma = 1$ gives the Fermi map [24, 14] for the Fermi acceleration mechanism for cosmic rays; $\gamma = 3/2$ gives the Kepler map [25, 26, 27, 28, 23] for a number of physical and astronomical applications; $\gamma = 2$ gives the “ultrarelativistic map” [15] for the motion of a relativistic particle in the field of a wave packet. All these maps describe dynamical behavior in the vicinities of separatrices

of corresponding models. In the case of the Kepler map the separatrix (the line $y = 0$) separates the bound and unbound states of motion.

The Kepler map (Eqs. (4) or (5) with $\gamma = 3/2$) was derived and analyzed in [25, 26, 27, 28] in order to describe the chaotic motion of the Halley comet and, generally, the motion of comets in highly eccentric orbits. The motion model for the Kepler map consists in the assumption that the main perturbing effect of planets (Jupiter first of all) is concentrated when the comet is close to the perihelion of its orbit. The y variable has the meaning of the normalized orbital energy of the comet, while x is the normalized time. One iteration of the map corresponds to one orbital revolution of the comet. This means that the map time unit, corresponding to one iteration, is not constant. The increment of real time per iteration is $\Delta x_i = x_i - x_{i-1}$.

The Kepler map is known to describe dynamics in several different settings of an hierarchical restricted three-body problem: in the external restricted planar [25, 26, 28] and strongly non-planar [29] problems in cometary dynamics; also in the abstract Sitnikov problem, where the tertiary moves along the *perpendicular* to the orbital plane of the main binary. The validity of the map in the last case follows from the work by Urminsky and Heggie [9], who considered a variant of the Sitnikov problem and derived a map (see Eqs. (11) in [9]), describing the dynamics in this problem. This map is straightforwardly reducible to the Kepler map (4); in particular, using formulas given in [9] for the parameters of their map, it is easy to derive a formula for the parameter λ in Eqs. (4):

$$\lambda = 2\pi(2.029e)^{-3/2} \approx 2.17e^{-3/2}, \quad (6)$$

where e is the eccentricity of the central binary. So, for the eccentricity e equal to 0.1 and 0.6 (chosen as representative in [9]) one has $\lambda \approx 70$ and 5, respectively. We choose these two values of λ for illustrative numerical experiments in what follows.

4 Lévy flights at the edge of escape: the distribution

The Lévy flights, i.e., the increments (in a kind of random walk) that have a heavy-tailed distribution, is a well-studied subject with various applications. In Hamiltonian dynamics, they were thoroughly considered in connection

with what we call the second kind Hamiltonian intermittency; see, e.g, [30] and references therein. In celestial mechanics, Lévy random walks arising due to close encounters of bodies were considered in the orbital energy evolution of comets [31].

Usually, Lévy flights are considered in random walks with steps possible in at least two (forward and back) directions; but the Lévy distributions considered below are one-sided: the increments (the orbital periods of the escaping body and the recurrence times) are positive. In a general statistical setting, one-sided Lévy flights were considered in [32, 33], where exact results for the first passage time and leapover statistics were obtained.

Both kinds of Lévy flights explored below in the framework of the three-body problem are *not* due to encounters of bodies. One of these two kinds is due to encounters of a trajectory with the separatrix in phase space; hereafter we call such flights the “Lévy flights of the first kind”, or LF1, since this phenomenon corresponds to the Hamiltonian intermittency of the first kind. Lévy flights of another kind, which we call the “Lévy flights of the second kind”, or LF2, are due to sticking of a trajectory to chaos border. In other words, these flights arise due to the second kind Hamiltonian intermittency. They effect the duration of long Poincaré recurrences, but not (practically) the orbital periods.

In the orbital behavior of the tertiary in the planar restricted three-body problem which we consider in what follows, the LF1 appear as sudden jumps in the orbital size and period, while LF2 appear as long sequences of orbital revolutions with almost constant orbital size and eccentricity.

LF1 still take place when encounters of bodies are impossible. E.g., in the cometary dynamics model, described by the Kepler map, [25, 26] the perihelion distance of the comet can be greater than the semi-major axis of the orbit of the secondary by any amount, but encounters with the separatrix with or without crossing it can still take place (if the cometary orbit is chaotic) and, as we shall see below, shape the statistics of recurrences.

In the dynamics of map (4), the LF1 and LF2 coexist (if λ is large enough, this condition is considered below). In Fig. 1, a fragment of a chaotic trajectory of map (4) with $\gamma = 3/2$ is shown, demonstrating LF1 (narrow peaks in the variation of the orbital period P_{orb} of the tertiary, on the left of the graph) and an LF2 (the oscillatory low “plateau” in the variation of y and P_{orb} , on the right). When y hits close to zero, a jump in the orbital period is observed. When the trajectory sticks to chaos border, both the energy and the orbital period oscillate near some low constant value.

The stickiness effect determines the character of the distribution of Poincaré recurrences on large timescales: it is algebraic [34, 35]. The algebraic decay in the recurrence statistics in Hamiltonian systems with divided phase space was considered, in particular, in [34, 35, 13, 36, 37], starting with a pioneering work by Chirikov and Shepelyansky [34]. Chirikov [13], using his resonant theory of critical phenomena in Hamiltonian dynamics, justified a value of $3/2$ for the critical exponent α in the integral distribution

$$F \propto T_r^{-\alpha} \tag{7}$$

of recurrences. The integral distribution $F(T_r)$ is defined here as the relative share of the recurrences with the duration greater than T_r in the whole sample. In a recent paper [37] the algebraic decay of Poincaré recurrences was explored statistically on the basis of large computational data on behavior of various Hamiltonian systems. These numerical experiments showed system-dependent power-law exponents, but the mean “universal” exponent turned out to be well-defined and equal to 1.57 ± 0.03 , somewhat differing from the standard $3/2$ value. Venegeroles [38] reports a value, equal to 1.54 ± 0.07 , resulting from averaging independent results of numerical studies of a number of various Hamiltonian systems; see Table 1 and references in [38].

In celestial mechanics, the algebraic decay was observed in numerical experiments on asteroidal dynamics [19, 20]. These experiments were performed in the framework of the restricted three-body problem Sun–Jupiter–asteroid. It was shown that the tail of the distribution of duration T_r of intervals between jumps of the orbital eccentricity of asteroids in the $3/1$ mean motion resonance with Jupiter is algebraic:

$$F \propto T_r^{-\alpha} \tag{8}$$

with $\alpha \approx 1.5$ – 1.7 typically. This was interpreted in [20] as an effect of sticking of the chaotic orbits to chaos border in the divided phase space. In other words, this is an effect of the second kind Hamiltonian intermittency.

On the other hand, Dones et al. [39] studied the escape times in the highly-eccentric chaotic cometary dynamics in the Solar system (the perturbations due to the four giant planets were taken into account) and reported on the algebraic tails of the integral distributions with the power-law index equal to 0.8 ± 0.2 . This behavior has not been theoretically interpreted up to now; we shall see that it can be straightforwardly interpreted as an effect of the first kind Hamiltonian intermittency.

The decay with $\alpha \approx 1.5$ is expected when LF2 dominate over LF1 in the long recurrences. A different kind of the decay law was observed in the behavior of the Kepler map by Borgonovi et al. [40]. They analyzed long-time decay properties of a Kepler map describing a one-dimensional model of hydrogen atom in a microwave field, and by means of rigorous deduction found a $T_d^{-2/3}$ law for the first approximation for the time decay of the survival probability in the case of the escape times measured in real (constant) time units. This law was confirmed by them in computed statistics; see Fig. 1 in [40]. On the opposite, when the escape times were measured in map (fictitious) time units, the usual $T_d^{-3/2}$ law was observed; see Fig. 2 in [40].

Apart from the rigorous treatment [40], several heuristic deductions of the $T_d^{-2/3}$ law are available in relevant problems [41, 42, 43]. Hut [42] derived an heuristic $T_d^{-2/3}$ law as a lower bound for the time decay of the survival probability in a general “hierarchical resonant scattering” [44, 42] setting for a three-body interaction (where the masses of “stars” are arbitrary). Malyshkin and Tremaine [43] derived the $T_d^{-2/3}$ law for the time decay of the survival probability for cometary ensembles in the Solar system. Schlagheck and Buchleitner [41] derived the $T_d^{-2/3}$ law for the time decay of the survival probability in an autoionizing configuration of chaotic helium.

In all these approaches, the $T_d^{-2/3}$ law was derived without using any Kepler map. Two basic assumptions were always made explicitly or implicitly, (i) that the distribution of ejection energies is flat or smooth in the neighborhood of the energy threshold $E = 0$, (ii) that the asymptotic decay of the survival probability is the same as the tail of the distribution of the orbital periods of the escaping body. While the first assumption is reasonable (in view of the complete ergodicity of the motion near the threshold, see analysis given below for the Kepler map), the second one is solely hypothetical. E.g., the argumentation presented in [43] is that the escaping comets “remain bound until their second perihelion passage, after which they will normally be ejected within a relatively short time”. However, given that all results [41, 42, 43] coincide with the result of the rigorous treatment in [40], we can infer that the second assumption seems to be also valid.

Let us, using the same two assumptions, find a law for the asymptotic distribution of the phase increments per iteration (which are the orbital periods of the escaping body in case of $\gamma = 3/2$) in the general case of arbitrary γ in map (4). The phase increment is

$$P = \Delta x_i = x_i - x_{i-1} = \lambda |y_i|^{-\gamma} \quad (9)$$

in real time units. In case of $\gamma = 3/2$ the real time unit is equal to the orbital period of the central binary, divided by 2π .

So, $|y_i| = \lambda^{1/\gamma} P^{-1/\gamma}$. The motion in the close vicinity of the separatrix is locally ergodic, i.e., regular islands are absent. This follows from the fact that in the local (in the energy y) approximation of map (4) by the standard map the stochasticity parameter of the standard map tends to infinity when y tends to zero. The ergodicity implies that, for the y variable close to zero, the distribution function of y is flat: $f(y) = \text{const}$. One has

$$\text{const } d|y| \propto P^{-\frac{1}{\gamma}-1} dP, \quad (10)$$

and the differential distribution function of P is

$$f(P) \propto P^{-\frac{1}{\gamma}-1}. \quad (11)$$

The integral distribution is $F(P) \propto P^{-\frac{1}{\gamma}}$.

For the Kepler map, $\gamma = 3/2$ and $P = P_{\text{orb}}$ (the orbital period); so, the differential distribution is $f(P_{\text{orb}}) \propto P_{\text{orb}}^{-5/3}$ and the integral distribution is $F(P_{\text{orb}}) \propto P_{\text{orb}}^{-2/3}$. From Kepler's third law one has $f(a) \propto a^{-2}$ for the differential distribution of the semi-major axis of the orbit; i.e., the distribution of the orbital size is also heavy-tailed, and the Lévy flights are demonstrated in the process of disruption both in tertiary's orbital period and size.

By assumption (ii), advocated above, law (11) coincides with the asymptotics of the time decay of the survival probability. Alternatively, the same law follows from repeating the analytical treatment [40] for the case of arbitrary γ instead of the exponent $3/2$ in the Kepler map: if one repeats the rigorous deduction [40] (performed in [40] for the Kepler map, $\gamma = 3/2$) in the general case of arbitrary γ , one finds the distribution $F(T_r) \propto T_r^{-\frac{1}{\gamma}}$ for the recurrence times. Note that the basic assumption in this deduction is that the phases are randomized after each kick.

Borgonovi et al. [40] explained the LF1 dominance over LF2 (in our terms) in real time statistics in the dynamics of the Kepler map, using argumentation based on the infinite measure of extended phase space near the separatrix. If one uses this argumentation in the general case of map (4) with arbitrary value of $\gamma > 0$, it follows that LF1 should dominate for all $\gamma \geq 1$ at least. However, while LF1 dominate indeed at $\gamma \geq 1$, the transition to this domination occurs at a value less than 1. Let us estimate this critical value. At $\gamma < \gamma_{\text{crit}}$, when LF2 dominate, the slope index is critical (in a different sense,

related to the “critical” structure at chaos border, see discussion above): $\alpha = \alpha_{\text{crit}} \approx 3/2$. At $\gamma > \gamma_{\text{crit}}$, when LF1 dominate, the slope index $\alpha = 1/\gamma$. These two curves $\alpha(\gamma)$ intersect at $\gamma = \gamma_{\text{crit}} = 1/\alpha_{\text{crit}} \approx 2/3$.

What is the physical reason for the switch to take place at this point? For the recurrences forming LF2 with duration greater than T , the “total sojourn time” $\sim TF(T)$ [36], i.e., $\sim T^{-\alpha_{\text{crit}}+1}$. Analogously, in the LF1 case, the total sojourn time is $\sim TF(T) \propto T^{-\frac{1}{\gamma}+1}$. LF1 asymptotically dominate, if the second sojourn time is greater than the first one: $T^{-\frac{1}{\gamma}+1} > T^{-\alpha_{\text{crit}}+1}$. Hence the condition for the LF1 domination is $\gamma > 1/\alpha_{\text{crit}}$. This is exactly what we have just derived for the point of intersection of the two curves $\alpha(\gamma)$.

So, a critical non-trivial value γ_{crit} of the γ parameter exists (if λ is large enough, see below), such as the maps with $\gamma > \gamma_{\text{crit}}$ have LF1 dominating over LF2 in real time statistics, whereas at $\gamma < \gamma_{\text{crit}}$ LF2 dominate in both the real time and map time statistics.

The quantity γ_{crit} equals $2/3$ in the case of the standard value $\alpha = 3/2$; and $\gamma_{\text{crit}} \approx 0.637$ in the case of $\alpha = 1.57$ computed in [37]. In particular, LF1 dominate over LF2 in real time statistics in the long Poincaré recurrences in the dynamics of the Fermi and Kepler maps, while for the ordinary separatrix maps, Markeev maps and \hat{L} -maps, if λ is large enough, the tails of the recurrence distributions are LF2-dominated and their slopes do not depend on the choice of units (map units or real time units) in which the lengths of recurrences are measured.

To illustrate the difference between distributions of recurrences measured in map and real time units, we present here examples of distributions obtained by iterating map (4) with $\gamma = 3/2$ (the Kepler map). In Fig. 2, the computed integral distributions $F(T_r)$ of the recurrence times T_r measured in map time units (iterations), are shown for $\lambda = 5$ (*bold line*) and $\lambda = 70$ (*thin line*). The number of iterations $n_{\text{it}} = 10^{11}$ in both cases. The recurrences are counted at the line $y = 0$. The quantity $F(T_r)$ is the fraction of recurrences longer than T_r . The tail of the distribution in Fig. 2 follows approximately the power law with the slope index $\alpha \approx 1.5$, as expected. It is similar, e.g., to the tails of distributions presented in Fig. 4 in [20] for the intervals between eccentricity bursts of chaotic asteroidal trajectories in the 3/1 Jovian resonance, where the same critical dynamical mechanism (sticking to chaos border) is present. In Fig. 3, the same distributions as in Fig. 2 are shown, but the recurrence times are measured in real time units. The slope index for the tails is evidently equal to $2/3$, as expected in this case. So, when real

time units are used, the tails of the distributions demonstrate a behavior that is different in slope and regularity, compared to the case of using the map time units. The reason is that LF1 dominate in the distribution tail in the first case, while LF2 dominate in the second case.

As we have already mentioned above, the LF1 and LF2 coexist in the dynamics of map (4), if λ is large enough. This condition provides the existence of the global fractal chaos border and, consequently, the prominent sticking phenomenon. If λ is small enough, map (4) can be reduced to a differential equation describing regular trajectories, at all y far from the separatrix $y = 0$. This can be done analogously to the case of the ordinary separatrix map (3); the procedure is described in [16]. Thus the motion far from the separatrix is locally regular, no global fractal chaos border exists; only LF1 are possible. This is the realm of “adiabatic chaos”.

What is the boundary value of λ , separating the cases with and without global fractal chaos border? It can be estimated from the form of the λ dependence of the maximum Lyapunov exponent L of map (4). The L value increases with λ , while λ is small, but then saturates at some constant value (see [45, fig. 3] for the Kepler map case $\gamma = 3/2$). The saturation takes place when the role of the global fractal chaos border becomes important in the dynamics. As follows from [45, fig. 3], the boundary value of λ for this map is ≈ 2 – 3 . In the case of the ordinary separatrix map, the transition value of λ is ≈ 0.5 – 1 (see [46, fig. 3], also [16, fig. 1]). By means of constructing the dependences $L(\lambda)$ for arbitrary $0 < \gamma < 2$, it can be shown that the boundary value of λ does not change much with γ and, by the order of magnitude, is ~ 1 . Thus, if $\lambda \gg 1$, we expect coexistence of LF1 and LF2 in the dynamics of map (4), while if $\lambda \ll 1$, only LF1 are possible.

Taking this into account (i.e., setting λ to be large enough), one can exploit the phenomenon of coexistence of LF1 and LF2 to estimate the value of the critical exponent α . Namely, one can compute the distribution functions (in real time) of the Poincaré recurrences for map (4) for a set of values of γ with some step, and, on increasing γ , fix its transition value γ_{crit} , when the tail of the integral distribution function starts to take the form characteristic for the LF1 statistics, i.e., the algebraic decay with the power-law index α equal to $1/\gamma$. Then $\alpha = 1/\gamma_{\text{crit}}$. Thus the procedure gives a new method for estimating the critical exponent α in Eq. (7). An example is given by the graphs in Fig. 4. One can see that the realization of our method with only two values of γ , namely, $\gamma = 1/2$ (corresponding to the \hat{L} -map) and $\gamma = 1$ (corresponding to the Fermi map), clearly shows that $1 < \alpha < 2$.

Now let us investigate this effect in more detail by building the dependence $\alpha(\gamma)$ directly, i.e., by finding α numerically on a grid of values of γ . When LF2 dominate, this dependence is expected to be subject to deformations arising due to marginal resonances at chaos border: at some intervals of γ , the border of the chaotic layer and, consequently, the recurrence statistics are perturbed due to emergence of the marginal resonances; on the marginal resonances, see [18]. In order to reduce maximally these perturbations, let us introduce a constant shift c in x in map (4), in the following way:

$$\begin{aligned} y_{i+1} &= y_i + \sin x_i, \\ x_{i+1} &= x_i + \lambda |y_{i+1}|^{-\gamma} + c. \end{aligned} \tag{12}$$

The shift c is a new parameter, analogous to the parameter c in map (3). At each value of γ we adjust the value of c in such a way that the winding number of the last undestroyed global KAM curve at the border of the chaotic layer is approximately equal to the “golden mean” $(5^{1/2} - 1)/2$; in other words, it is maximally far from the main resonances.

By means of linearization of map (4) or (12) in y it is straightforward to see that the value of y corresponding to the critical value of the stochasticity parameter $K = K_G \approx 0.971635406$ [12, 14, 48] of the approximating standard map is $y_b = (\gamma\lambda/K_G)^{\frac{1}{\gamma+1}}$. This value corresponds to the border of the chaotic layer. The regularizing constant shift c is found by averaging the phase increment at the border of the chaotic layer; the resulting formula is

$$c_{\text{reg}} = \pi(5^{1/2} - 1) - \lambda(\gamma\lambda/K_G)^{-\gamma/(\gamma+1)}. \tag{13}$$

Since the form of the relationship $\alpha(\gamma)$ is expected to be independent from λ , when λ is large enough, one can take any large value $\lambda \gg 1$; we choose $\lambda = 10$. We build the graph on the interval $0 < \gamma \leq 2$ with the resolution $\Delta\gamma = 0.01$, i.e., we make 200 measurements of α . At each value of γ on the grid, the integral distribution built in logarithmic coordinates is linearly fitted on the interval $3 < \log_{10} T_r < 6$; T_r is measured in real time units. The left border of the interval is chosen to be much greater than the point of transition from the initial behavior (which can be exponential or inverse square-root, see [36]) to the asymptotic one. A direct inspection of the constructed distributions shows that this transition occurs at $\log_{10} T_r < 2$ for all points on the γ grid. The right border of the T_r interval is defined to be much less than the values at which the distributions exhibit a drop due

to poor statistics at the very tails. At each point on the γ grid, the number of iterations of the map is $n_{\text{it}} = 10^{10}$.

In Fig. 5, the computed dependence $\alpha(\gamma)$ is shown for two cases, $c = 0$ and $c = c_{\text{reg}}$. The *bold line* corresponds to the map with $c = c_{\text{reg}}$, whereas the *thin line* corresponds to the map with $c = 0$. One can see that in the first case the irregular perturbations of the dependence are indeed suppressed seriously, though they are not at all completely eliminated. In the both cases, the transition to the LF1 domination at $\gamma \approx 0.7$ is evident, in agreement with our prediction. However, it is also evident that the numerical construction of the $\alpha(\gamma)$ dependence does not provide a high-precision tool for determining the α_{crit} value, because the perturbations of the theoretically “flat” behavior at $\gamma < \gamma_{\text{crit}}$ are large, and, due to them, the transition point cannot be located precisely. What is more, the suppression of the border perturbations by adjustment of the c parameter might introduce systematic errors (yet unexplored theoretically) in the estimated value of α_{crit} .

Another way seems to be much more promising here. To locate the transition point, one can exploit the property of fluctuations of the recurrence time distribution in the case of the second kind Hamiltonian intermittency, as opposed to the perfectly unperturbed behavior in the case of its first kind (see Figs. 4). In our fits of the T_r distributions, the α values are determined with their standard errors, i.e., at each point of γ one obtains $\alpha \pm \sigma$ as an estimate for the power-law index. In Fig. 6, high-resolution γ dependences of the standard deviation σ for the numerically determined power-law index α are shown for $\lambda = 5$ (*lower line*) and $\lambda = 10$ (*upper line*); $c = c_{\text{reg}}$. The interval of γ is taken to be in the neighborhood of the expected switch value; namely, $0.55 \leq \gamma \leq 0.80$. The resolution of the plot in γ is $\Delta\gamma = 0.0005$. All other details of the numerical procedure are the same as adopted for construction of Fig. 5.

In the constructed dependences in Fig. 6, a transition from a linear decline from large values of σ to a low-level horizontal plateau takes place in a narrow interval $\approx 0.67 < \gamma < \approx 0.68$ (corresponding to $\alpha_{\text{crit}} \approx 1.5$), in agreement with our prediction for the critical value of γ . Concluding, construction and analysis of the dependence $\sigma(\gamma)$ does indeed provide a perspective numerical tool for determining the α_{crit} value.

5 Lévy flights at the edge of escape: the “ T_L — T_r ” relation

As discussed in the Introduction, the power-law character of the dependence of the times of sudden orbital changes on the Lyapunov times [1, 2, 3, 4, 5, 6, 7] was explained in [6, 11] as a phenomenon of critical dynamics, i.e., an effect of motion near chaos border. This is an effect of the second kind Hamiltonian intermittency.

Here we show that the first kind Hamiltonian intermittency in the three-body problem at the edge of disruption leads to a quasilinear “ T_L — T_r ” relation, when the times are measured in real time units. As follows from Eqs. (4), the length of a Poincaré recurrence in real time units is

$$T_r^{(\text{ru})} = \sum_{i=1}^n \Delta x_i = \lambda \sum_{i=1}^n |y_i|^{-3/2}, \quad (14)$$

where $n = T_r$ is the duration of the Poincaré recurrence in map time units (iterations); the time increment $\Delta x_i = x_i - x_{i-1}$, and the iteration $i = 1$ is set for the start of the recurrence.

Let us consider the finite-time maximum Lyapunov exponent (of an original dynamical system) calculated for a recurrence in the case when real time units are used. To obtain it, one should divide the calculated finite-time maximum Lyapunov exponent L of the map by the average (on the recurrence) length $\langle P_{\text{map}}^{(\text{ru})} \rangle = T_r^{(\text{ru})}/T_r$ of the map iterations in real time (see, e.g., [14]). Hereafter we denote $\langle P_{\text{map}}^{(\text{ru})} \rangle$ by q :

$$q = \frac{T_r^{(\text{ru})}}{T_r} = \frac{1}{n} \sum_{i=1}^n \Delta x_i = \frac{\lambda}{n} \sum_{i=1}^n |y_i|^{-3/2}. \quad (15)$$

The maximum Lyapunov exponent referred to real time units is

$$L^{(\text{ru})} = \frac{L}{q}. \quad (16)$$

Equivalently, for the Lyapunov time one has

$$T_L^{(\text{ru})} = qT_L. \quad (17)$$

On the other hand,

$$T_r^{(\text{ru})} = qT_r. \quad (18)$$

The quantity $q = T_r^{(\text{ru})}/T_r$ is the ratio of two random variables, distributed as power laws, as shown above. If the y value hits close to the separatrix, then, according to (14), there is a jump in $T_r^{(\text{ru})}$, but there is no jump in T_r . If the magnitude of such jumps is much greater than the total range of the original “ $T_L - T_r$ ” graph in map time units (this is the case when LF1 dominate over LF2), the graphical relationship in real time units will be spread, due to the jumps, in the direction $T_L = T_r$. So, when T_L and T_r are expressed in real time units and LF1 dominate over LF2, the “ $T_L - T_r$ ” relationship becomes quasilinear.

This inference is valid when LF1 dominate. For the ordinary separatrix map (3) and general maps (4) with $\gamma < \gamma_{\text{crit}}$, where singularity is weaker, LF2 dominate if λ is large enough, and the generic relationship is not spread in the $T_L = T_r$ direction. This is the reason why the close-to-quadratic relationship [1, 2, 3, 4, 5, 6, 7], and not the quasilinear one, is present in the dynamics of minor Solar system bodies near resonances, where the ordinary separatrix map, but not the Kepler map, is relevant to the dynamics of interacting nonlinear resonances.

To illustrate our theoretical inferences, let us compute the “ $T_L - T_r$ ” relationships for the Kepler map in map time units (iterations) and, for comparison, in real time units. The finite-time maximum Lyapunov exponent is computed for a recurrence. In Fig. 7, the computed relationship in the map time units is shown for $\lambda = 5$, $n_{\text{it}} = 10^7$. One can see, that, judging by the general slope of the dependence in log-log scale, the dependence is far from being linear here. Its slope in log-log scale is much steeper: the power law index is equal to 1.5–2, as expected. Now let us measure the recurrence times in real time units. Apart from this change in the time units, the same (as in Fig. 7) dependence is built in Fig. 8. Now the relationship is evidently quasilinear, in accord with our theoretical finding for the case of real time units. One can even see how the “spreading” mechanism operates: the dependence has a “V” form, where the left wing is much shorter and represents a remnant (left after spreading by LF1) of the generic close-to-quadratic relationship. Thus the general “composite” appearance of the “ $T_L - T_r$ ” diagram (in real time units) for the Kepler map mimics general structure of the “ $T_L - T_r$ ” diagrams revealed in computations of the disruption process in the three-body problem in various settings; compare Fig. 8 with figures 2 and 3 in [8] or with figures 3 and 7 in [9].

The over-all appearance of the diagram in Fig. 7 looks rather irregular, in comparison with that in Fig. 8. The nature of this irregularity can be clarified

by means of construction of a spectrum of winding numbers [47]. It can be built here for the Kepler map analogously to construction of the spectrum for the ordinary separatrix map in [47]. The spectrum of winding numbers graphically demonstrates which of the resonant chains of islands produce the longest events of sticking. The winding number Q is formally defined for a recurrence as $Q = \Delta x/n$, where Δx is the length of a Poincaré recurrence (the duration of an interval between crossings of the separatrix), measured as the total sum of variations in the phase x taken modulo 2π , and $n = T_r$ is the length of the Poincaré recurrence measured in the map iterations. We build the spectrum of winding numbers by plotting $\log_{10} n$ versus Q . In Fig. 9, the spectrum of winding numbers computed for $\lambda = 5$ and $n_{it} = 5 \cdot 10^{11}$ is shown. The Farey tree [48] of resonances is evident. Consider some lowest order resonances m/n and m'/n' that are “neighboring”, i.e., $mn' - m'n = 1$, then the lower level of the tree is made of “mediants” given by the formula $m''/n'' = (m + m')/(n + n')$. In Fig. 9, the evident lowest order resonances are $1/7$, $1/6$ and $1/5$. The mediants for them are $2/13$ and $2/11$. For the resonances $1/7$ and $2/13$ the mediant is $3/20$; for the resonances $2/13$ and $1/6$ the mediant is $3/19$; and so on. All mentioned resonances produce visible peaks and are easily identified in Fig. 9. We see that the irregular structure in Fig. 7 is explained by overlapping of individual relationships for several sticky island chains. The overlap of these relationships at the given timescale of recurrences produces the observed irregularity.

6 Range of applicability

Let us consider in more detail the range of applicability of the presented results on the statistics of the disruption process. Clearly, these results are valid wherever the Kepler map (4) description of the motion of the tertiary is valid. First of all, we assume that the orbit of the escaping body is highly eccentric, and its pericenter distance q is much greater than the size of the orbit of the main binary.

Hence the inferred statistics of the disruption and Lyapunov times are expected in an hierarchical restricted three-body problem, where the pericenter distance of the tertiary is much greater than the size of the orbit of the main binary. The eccentricity of the orbit of the main binary as well as the non-coplanarity of the three-body system do not play role due to the following reasons. As it has been already mentioned above, the Kepler map is known to

describe the highly eccentric motion of a tertiary in several different settings of an hierarchical restricted three-body problem: in the external restricted planar and strongly non-planar problems, also in the Sitnikov problem. If the pericenter distance is large enough, only one harmonic in the Fourier expansion of the energy increment is important and is enough to be taken into account [28, 49].

A role of the mass parameter μ in the main binary has not been explored yet, but one may expect the validity of the Kepler map approximation for the motion again, when q is large, because the higher order harmonics in the energy increment expansion are exponentially small with q [28, 49]. Moreover, the formula for the energy increment in Eqs. (5) in the case of the circular-orbit main binary with the mass parameter $\mu = 1/2$ (equal-mass binary) is similar to that in the case of the circular-orbit main binary with small μ . To clarify this point, let us compare the formulas. In the circular planar restricted three-body problem with small μ one has for the energy increment, if $q \gg 1$ (q is measured in the units of the semi-major axis of the main binary):

$$\Delta w \equiv w_{i+1} - w_i \propto \mu q^{-1/4} \exp\left(-\frac{2^{3/2}q^{3/2}}{3}\right) \sin \tau_i \quad (19)$$

in the case of prograde orbits of the tertiary, and

$$\Delta w \propto \mu q^{-7/4} \exp\left(-\frac{2^{3/2}q^{3/2}}{3}\right) \sin \tau_i \quad (20)$$

in the case of retrograde orbits of the tertiary [28, formulas (3.16)]. In the case of the equal-mass main binary and the non-planar problem, it can be found from [50, formula (26)] in the restricted problem limit that

$$\Delta w \propto q^{3/4} \exp\left(-\frac{2^{5/2}q^{3/2}}{3}\right) \cos^4 \frac{I}{2} \sin 2\tau_i, \quad (21)$$

where I is the inclination of tertiary's orbit. We see that the structure of the formulas is similar, putting aside some differences in the numerical values of the coefficients and the power-law indices. Note that formulas (19, 20, 21) can be used, if necessary, to find numerical values of the λ parameter in Eqs. (4), because these formulas provide estimates of the W parameter in Eqs. (5), while the formula for κ in Eqs. (5) is trivial (it is simply the time normalization, see, e.g., [28]).

The inferred statistics appear to be still valid in a more general “hierarchical resonant scattering” [44, 42] setting for a three-body interaction, where the masses of “stars” are arbitrary. Hut [42] derived an heuristic $T_d^{-2/3}$ law as a lower bound for the time decay of the survival probability in this setting, and showed this law to describe well the tails of numerical-experimental distributions. Note that this heavy-tailed distribution is in accord with an early finding by Agekian et al. [51] that the mean life-time of a general isolated three-body system is infinite.

As we have seen above, two basic assumptions are necessary for heuristic derivation of the $T_d^{-2/3}$ law, namely, (i) that the distribution of ejection energies is smooth in the neighborhood of the energy threshold $E = 0$, (ii) that the asymptotic decay of the survival probability is the same as the tail of the distribution of the orbital periods of the escaping body. These two assumptions look rather plausible even in the general three-body problem. Combining these considerations and our theoretical findings described above, we see that the $T_d^{-2/3}$ law is expected to be quite universal.

However, neither the $T_d^{-2/3}$ law, nor even any other algebraic law were reported in the numerical-experimental studies in [8, 9]. We think that the main reasons are that the algebraic fitting functions were not used, and, besides, solely the initial part of the distribution was built in [8], though the time range of the simulations allowed one to study the tails. Another point is that the tail of the disruption time distribution in the given problem should be considered separately from the initial part, because it corresponds to a different dynamical situation: here the regime of decay might be Poissonian (see analogues in [19, 20, 11]), or, in the very beginning, inverse square-root [34, 36, 11].

Our theoretical inferences seem to be confirmed by the results of the very recent study [52], where the statistics of the decay process in the equal-mass three-body problem with randomized initial conditions were investigated in extensive numerical experiments. The lifetime distributions obtained in [52] have turned out to be heavy-tailed, i.e., the tails have turned out to be algebraic. The computed power-law index α for the integral distribution has been found to be within the narrow range, approximately from 0.4 to 0.7, depending on the virial coefficient (see [52]). The theoretically predicted value $\alpha = 2/3$ is within this narrow range.

The range of applicability of the derived “ $T_L - T_d$ ” relationship is similar to that of the derived distribution law. The proximity of our theoretical

quasilinear “ $T_L - T_d$ ” relationship to the numerical-experimental results in [8] (obtained for an equal-mass three-body system) has a natural heuristic explanation, consisting in that the stage before disruption is hierarchical, with the outer body exhibiting the usual final Lévy flights, and this process can be described in the “hierarchical resonant scattering” setting for a three-body interaction (though, in general, triple encounters can play role).

Finally, there is no wonder that a simple one-parameter two-dimensional map, such as the Kepler map, is able to describe the essential dynamics of disruption of a system with several degrees of freedom. The matter is that we consider a very special stage of the system evolution subject to serious limitations: the orbit of the escaping body is highly eccentric, and its pericenter distance is much greater than the size of the main binary. In many respects, reduction of the motion to the Kepler map in the problem considered is similar to reduction of the motion in the vicinity of the separatrices of the “guiding resonance” to the separatrix map (see [12]) in a general Hamiltonian system. An important difference, however, is that the ordinary separatrix map has two parameters, and cannot be reduced, opposite to the case of the Kepler map, to a one-parameter form, because the phase increment in the ordinary separatrix map is logarithmic.

7 Conclusions

We have considered statistics of the disruption and Lyapunov times in an hierarchical restricted three-body problem. As we have seen, at the edge of escape the orbital periods of the escaping body exhibit Lévy flights. Due to them, the distribution of the disruption times is heavy-tailed with the power-law index of the integral distribution equal to $-2/3$, while the relation between the Lyapunov and disruption times is quasilinear. The former finding is in accord with heuristic and numerical-experimental results in [41, 42, 43], while the latter one is in accord with recent numerical-experimental results in [8, 9]. Our theoretical results are valid for any system described by the Kepler map, i.e., they are valid at least in the external restricted three-body problem, both planar and non-planar, where the tertiary does not suffer close encounters with the central binary. The derived statistical laws appear to be valid as well in a more general “hierarchical resonant scattering” setting for a three-body interaction.

The sharp difference between the two kinds of Hamiltonian intermittency,

in what concerns the slope indices of the asymptotic power-law distributions of the Poincaré recurrences, allows one to explain the observed difference in the power-law indices of the distribution laws reported for the chaotic dynamics of the Solar system minor bodies. Dones et al. [39] reported on the algebraic tails of the integral distributions with the power-law index α equal to 0.8 ± 0.2 , whereas Shevchenko and Scholl [19, 20] reported on the tails with the index equal to ≈ 1.5 . In [39] the escape times in the highly-eccentric chaotic cometary dynamics in the Solar system were studied (the perturbations due to the four giant planets were taken into account), whereas in [19, 20] the subject was the low-eccentricity intervals between the eccentricity jumps in the chaotic asteroidal dynamics (in the restricted three-body problem Sun–Jupiter–asteroid). Judging by the values of the power-law index, the former statistics correspond to the Hamiltonian intermittency of the first kind, whereas the latter one to that of the second kind. The statistics are LF1-dominated and LF2-dominated, respectively, and the predicted power-law indices α are respectively equal to $2/3$ and $\approx 3/2$. The evident “inverse symmetry” of the indices is a property of the gravitational dynamics, described by the Kepler map; generally, when a separatrix map with an arbitrary γ is in action, the predicted indices are $1/\gamma$ and $\approx 3/2$, respectively. Thus the latter index is more “universal” than the former one.

The change of the power-law index value (≈ 1 instead of ≈ 2) in the “ $T_L - T_d$ ” relationship in comparison with the results on the dynamics of the Solar system minor bodies obtained in [1, 2, 3, 4, 5, 6, 7] is due to the fact that the singularity at crossing the separatrix is much stronger in the considered problem (which is described by the Kepler map instead of the ordinary separatrix map), and therefore the first kind Hamiltonian intermittency dominates over its second kind and thus defines the properties of the “ $T_L - T_d$ ” relationship and the tail of the disruption time distribution.

We have shown that a critical non-zero value γ_{crit} of the γ parameter of general map (4) exists that separates the maps with LF2-dominated dynamics from those with LF1-dominated dynamics.

As a by-product of our study we have proposed a new method for estimating the critical exponent α in Eq. (7). This method is based on computation of the γ transition value separating maps (4) with LF1-dominated and LF2-dominated statistics of long recurrences.

Finally, our inferences shed light on the mechanism of disruption of an hierarchical three-body system in the adopted setting of the problem: the typical way of disruption, as described by the Kepler map, is a kind of “Lévy

unfolding” of the system in both time and space: at the edge of the system’s disruption, the escaping body exhibits Lévy flights in its orbital period and semi-major axis, and in the course of this random process the orbital period and semi-major axis become arbitrarily large until the separatrix separating the bound and unbound states of the motion is crossed and the body escapes.

Acknowledgments

The author is thankful to V. V. Orlov and anonymous referees for valuable remarks and comments. This work was partially supported by the Russian Foundation for Basic Research (projects # 09-02-00267 and # 10-02-00383) and by the Programme of Fundamental Research of the Russian Academy of Sciences “Fundamental Problems in Nonlinear Dynamics”.

References

- [1] M. Soper, F. Franklin, and M. Lecar, *Icarus* **87**, 265 (1990).
- [2] M. Lecar, F. Franklin, and M. Murison, *Astron. J.* **104**, 1230 (1992).
- [3] M. A. Murison, M. Lecar, and F. A. Franklin, *Astron. J.* **108**, 2323 (1994).
- [4] H. F. Levison and M. J. Duncan, *Astrophys. J. Lett.* **406**, L35 (1993).
- [5] S. Ferraz-Mello, *Celest. Mech. Dyn. Astron.* **65**, 421 (1997).
- [6] I. I. Shevchenko, *Phys. Lett. A* **241**, 53 (1998).
- [7] K. Tsiganis, H. Varvoglis, and R. Dvorak, *Celest. Mech. Dyn. Astron.* **92**, 71 (2005).
- [8] S. Mikkola and K. Tanikawa, *Mon. Not. R. Astron. Soc.* **379**, L21 (2007).
- [9] D. J. Urminsky and D. C. Heggie, *Mon. Not. R. Astron. Soc.* **392**, 1051 (2008).
- [10] K. A. Sitnikov, *Sov. Phys. Doklady* **5**, 647 (1960). [Dokl. Akad. Nauk USSR **133**, 303 (1960).]

- [11] I. I. Shevchenko, in: *Impact of Modern Dynamics in Astronomy*, edited by J. Henrard and S. Ferraz-Mello (Kluwer, Dordrecht, 1999) 383.
- [12] B. V. Chirikov, Phys. Reports **52** (1979) 263 (1979).
- [13] B. V. Chirikov, *Patterns in chaos*. INP Preprint 90–109 (Institute of Nuclear Physics, Novosibirsk, 1990).
- [14] A. J. Lichtenberg and M. A. Leiberman, *Regular and Chaotic Dynamics* (Springer-Verlag, New York, 1992).
- [15] G. M. Zaslavsky, R. Z. Sagdeev, D. A. Usikov, and A. A. Chernikov, *Weak Chaos and Quasi-Regular Patterns* (Cambridge University Press, Cambridge, 1991).
- [16] I. I. Shevchenko, Phys. Lett. A **372**, 808 (2008).
- [17] I. I. Shevchenko, Mon. Not. R. Astron. Soc. **384**, 1211 (2008).
- [18] I. I. Shevchenko, Physica Scripta **57**, 185 (1998).
- [19] I. I. Shevchenko and H. Scholl, in: *Dynamics, Ephemerides and Astrometry of the Solar System*, edited by S. Ferraz-Mello, B. Morando, and J.-E. Arlot (Kluwer, Dordrecht, 1996) 183.
- [20] I. I. Shevchenko and H. Scholl, Celest. Mech. Dyn. Astron. **68**, 163 (1997).
- [21] A. P. Markeev, Prikl. Mat. Mekh. **59**, No. 4, 569 (1995). [In Russian.]
- [22] A. P. Markeev, Prikl. Mat. Mekh. **58**, No. 5, 37 (1994). [In Russian.]
- [23] S. S. Abdullaev, *Construction of Mappings for Hamiltonian Systems and Their Applications* (Springer, Berlin, Heidelberg, 2006).
- [24] G. M. Zaslavsky and B. V. Chirikov, Sov. Phys. Doklady **9**, 989 (1965). [Dokl. Akad. Nauk USSR **159**, 306 (1964).]
- [25] T. Y. Petrosky, Phys. Lett. A **117**, 328 (1986).
- [26] B. V. Chirikov and V. V. Vecheslavov, *Chaotic Dynamics of Comet Halley*. INP Preprint 86–184 (Institute of Nuclear Physics, Novosibirsk, 1986).

- [27] V. V. Vecheslavov and B. V. Chirikov, *Sov. Astron. Lett.* **14**, 151 (1988). [*Pis'ma Astron. Zh.* **14**, 357 (1988).]
- [28] T. Y. Petrosky and R. Broucke, *Celest. Mech. Dyn. Astron.* **42**, 53 (1988).
- [29] V. V. Emelyanenko, *Sov. Astron. Lett.* **16**, 318 (1990) [*Pis'ma Astron. Zh.* **16**, 737 (1990)]
- [30] S. Denisov, J. Klafter, and M. Urbakh, *Phys. Rev. E* **66**, 046217 (2002).
- [31] J. Zhou, Y. Sun, and L. Zhou, *Celest. Mech. Dyn. Astron.* **84**, 409 (2002).
- [32] T. Koren, J. Klafter, and M. Magdziarz, *Phys. Rev. E* **76**, 031129 (2007).
- [33] T. Koren, M. A. Lomholt, A. V. Chechkin, J. Klafter, and R. Metzler, *Phys. Rev. Lett.* **99**, 160602 (2007).
- [34] B. V. Chirikov and D. L. Shepelyansky, *Statistics of Poincaré Recurrences and the Structure of the Stochastic Layer of the Non-linear Resonance*. INP Preprint 81–69 (Institute of Nuclear Physics, Novosibirsk, 1981). [In Russian.]
- [35] B. V. Chirikov and D. L. Shepelyansky, *Physica D* **13**, 395 (1984).
- [36] B. V. Chirikov, *Poincaré Recurrences in Microtron and the Global Critical Structure*. INP Preprint 99–7 (Institute of Nuclear Physics, Novosibirsk, 1999) [eprint arXiv:nlin/0006013].
- [37] G. Cristadoro and R. Ketzmerick, *Phys. Rev. Lett.* **100**, 184101 (2008).
- [38] R. Venegeroles, *Phys. Rev. Lett.* **102**, 064101 (2009).
- [39] L. Dones, H. F. Levison, and M. Duncan, in: *Completing the Inventory of the Solar System*, edited by T. W. Rettig and J. M. Hahn, ASP Conference Series (Astron. Soc. Pacific, San Francisco, 1996), vol. 107, 233.
- [40] F. Borgonovi, I. Guarneri, and P. Sempio, *Nuovo Cimento Soc. Ital. Fis. B* **102**, 151 (1988).

- [41] P. Schlagheck and A. Buchleitner, *Phys. Rev. A* **63**, 024701 (2001).
- [42] P. Hut, *Astrophys. J.* **403**, 256 (1993).
- [43] L. Malyskin and S. Tremaine, *Icarus* **142**, 341 (1999).
- [44] D. C. Heggie, *Mon. Not. R. Astron. Soc.* **173**, 729 (1975).
- [45] I. I. Shevchenko, In: *Near Earth Objects, our Celestial Neighbors: Opportunity and Risk*, edited by A. Milani, G. B. Valsecchi, and D. Vokrouhlický (Cambridge Univ. Press, Cambridge, 2007) 15.
- [46] I. I. Shevchenko, *JETP Letters* **79**, 523 (2004) [*Pis'ma Zh. Eksp. Teor. Fiz.* **79**, 651 (2004)].
- [47] I. I. Shevchenko, In: *Chaos in Gravitational N-Body Systems*, edited by J. C. Muzzio, S. Ferraz-Mello, and J. Henrard (Kluwer, Dordrecht, 1996) 311.
- [48] J. D. Meiss, *Rev. Mod. Phys.* **64**, 795 (1992).
- [49] J. Liu and Y. S. Sun, *Celest. Mech. Dyn. Astron.* **60**, 3 (1994).
- [50] A. Roy and M. Haddow, *Celest. Mech. Dyn. Astron.* **87**, 411 (2003).
- [51] T. A. Agekian, Zh. P. Anosova, and V. V. Orlov, *Astrophysics* **19**, 66 (1983).
- [52] V. V. Orlov, A. V. Rubinov, and I. I. Shevchenko, eprint arXiv:1004.2506 (2010).

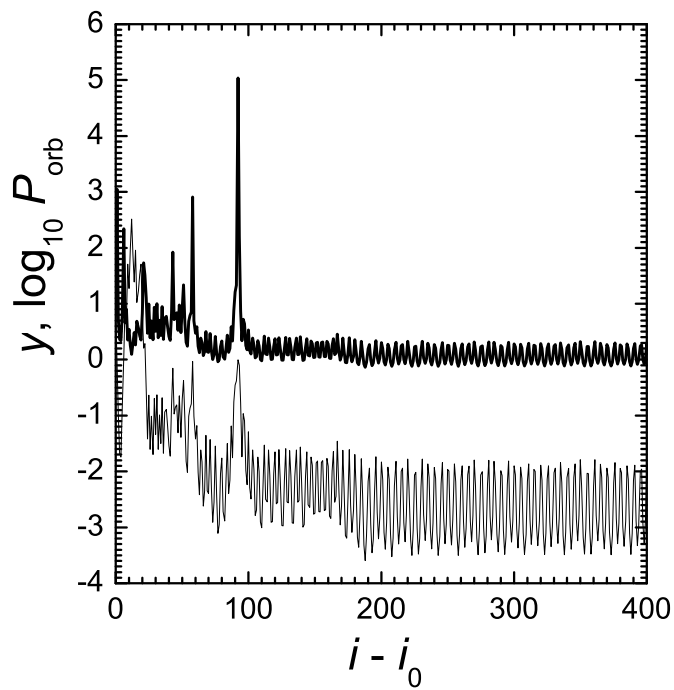


Figure 1: A fragment of a chaotic trajectory of the Kepler map, demonstrating Lévy flights of the first kind (the prominent peaks of $\log_{10} P_{\text{orb}}$ on the left) and a Lévy flight of the second kind (the oscillatory “plateau” of y and $\log_{10} P_{\text{orb}}$ on the right). y is shown with a thin line, and $\log_{10} P_{\text{orb}}$ with a bold one; $\lambda = 5$; the value of i_0 is some big number chosen to exhibit this part of trajectory.

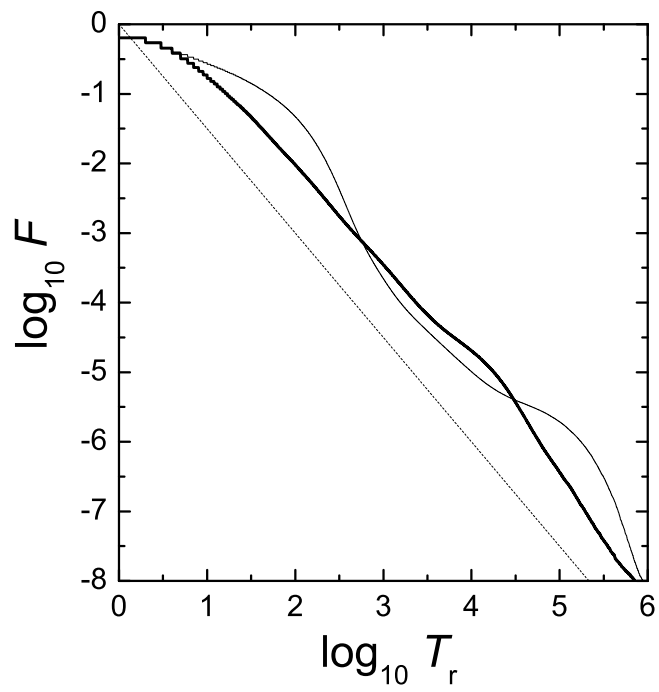


Figure 2: Integral distributions of the recurrence times measured in map time units (iterations) for the Kepler map; $\lambda = 5$ (*bold line*) and $\lambda = 70$ (*thin line*). The straight dotted line shows the $T_r^{-3/2}$ law.

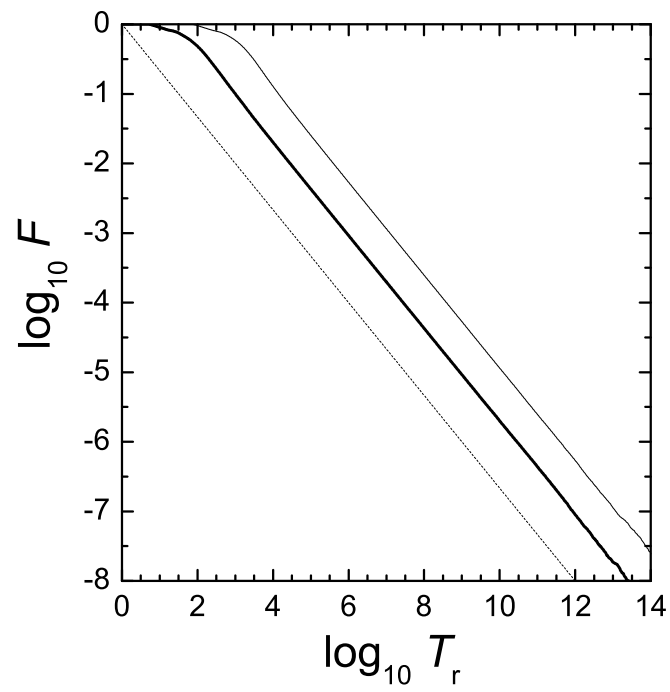
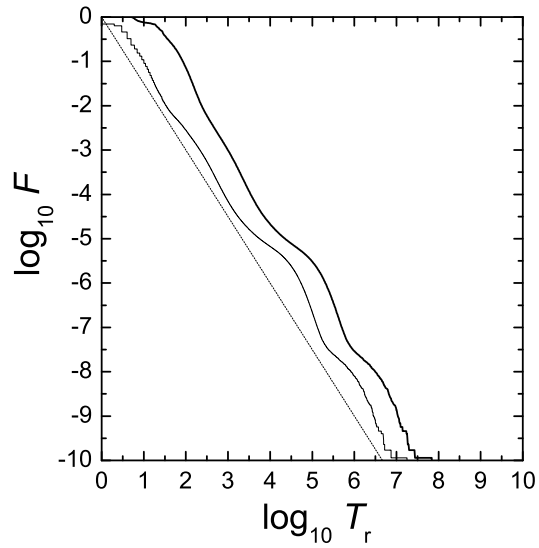
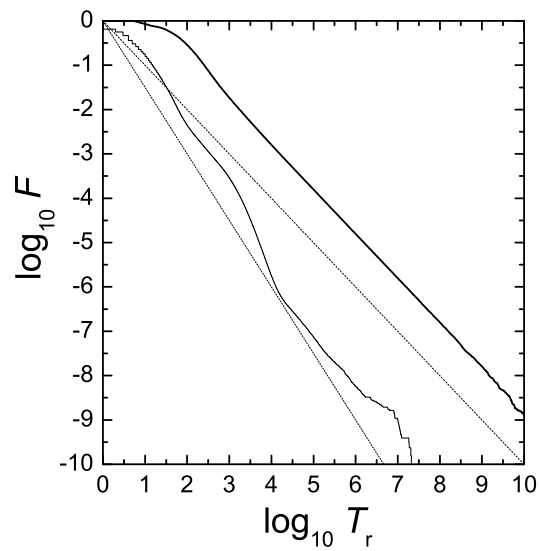


Figure 3: The same as in Fig. 2, but the recurrence times are measured in real time units. The bold line corresponds to $\lambda = 5$, and the thin one to $\lambda = 70$. The straight dotted line shows the $T_r^{-2/3}$ law.



a)



b)

Figure 4: Integral distributions of the recurrence times measured in real time (*bold lines*) and map time (*thin lines*) units for the \hat{L} -map (a) and for the Fermi map (b); $\lambda = 5$; $n_{it} = 10^{11}$. The straight dotted lines show the $T_r^{-3/2}$ and T_r^{-1} laws.

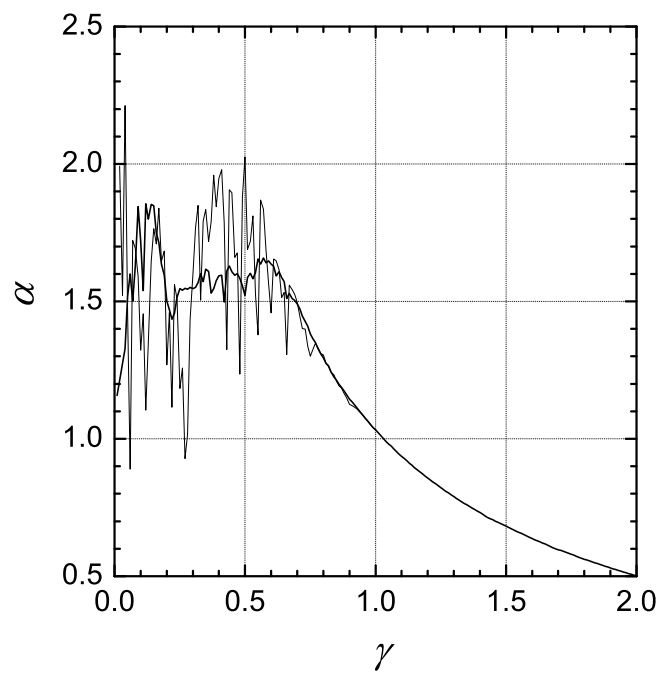


Figure 5: The dependence of the computed power-law index α on the γ parameter, for $c = c_{\text{reg}}$ (bold line) and $c = 0$ (thin line); $\lambda = 10$.

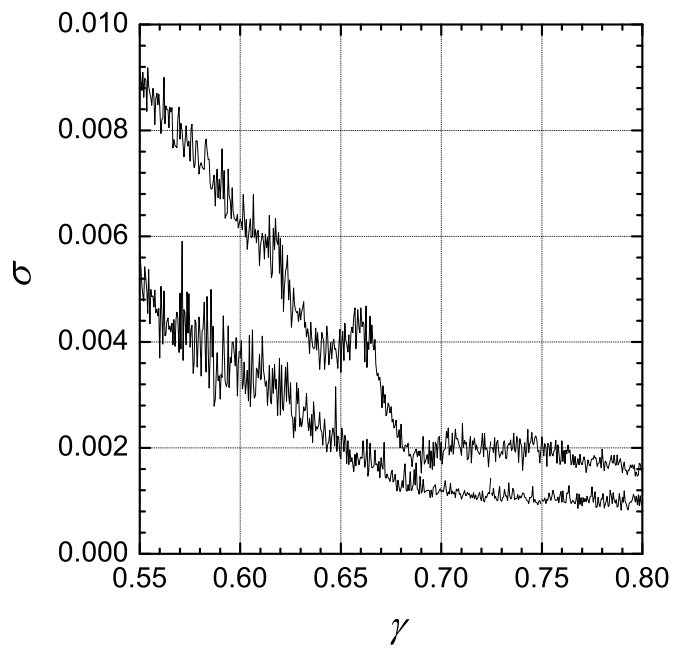


Figure 6: The γ dependence of the standard deviation σ for the computed power-law index α ; $\lambda = 5$ (lower line) and $\lambda = 10$ (upper line); $c = c_{\text{reg}}$.

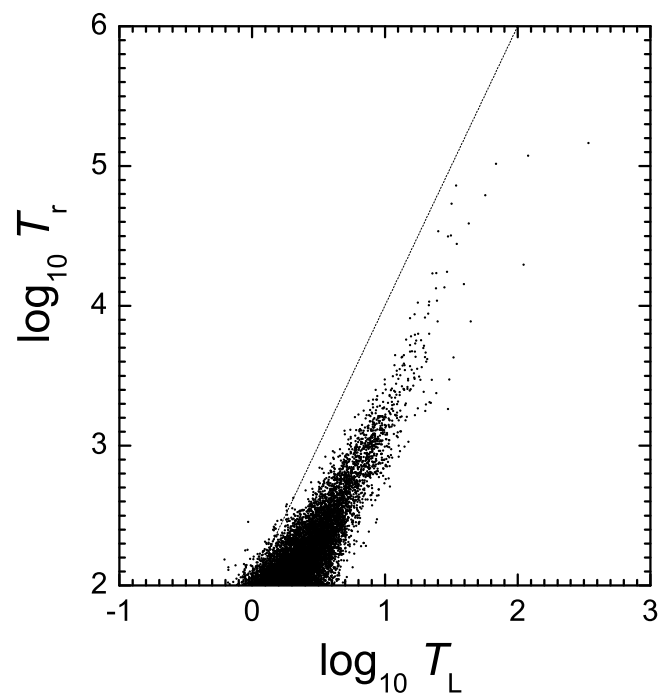


Figure 7: A statistical relation “ $\log_{10} T_L - \log_{10} T_r$ ”, where T_L and T_r are measured in map time units; $\lambda = 5$. The straight dotted line shows the quadratic dependence.

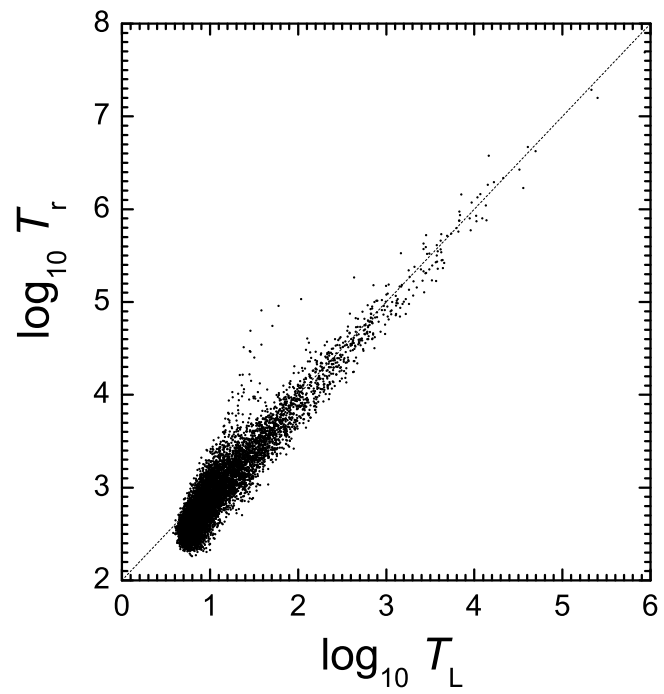


Figure 8: The same as in Fig. 7, but the recurrence times are measured in real time units. The straight dotted line shows the linear dependence.

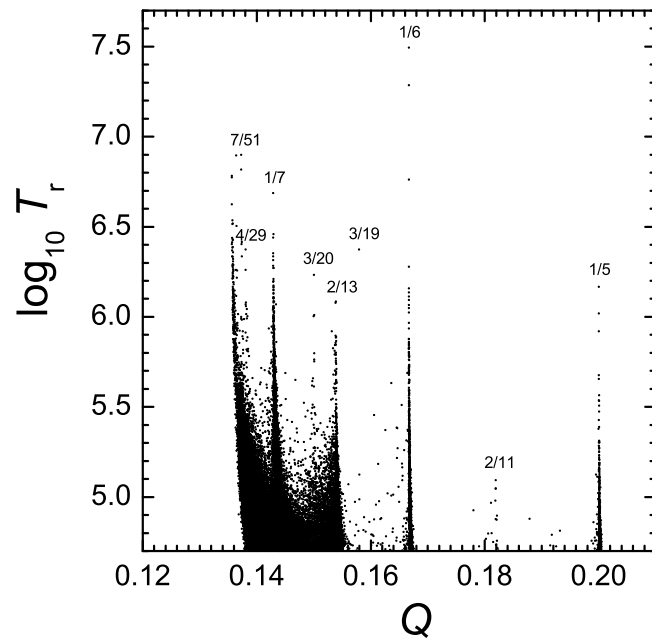


Figure 9: A spectrum of winding numbers, visualizing the resonant structure of the chaotic motion near chaos border; $\lambda = 5$.